Effects of a sheath boundary on electron energy distribution in Ar/He dc magnetron discharges

ARTICLE *in* JOURNAL OF APPLIED PHYSICS · JUNE 2004

Impact Factor: 2.18 · DOI: 10.1063/1.1755850

3 AUTHORS, INCLUDING:

Sang Hun Seo
Korea Advanced Institute of Science and Tec…
36 PUBLICATIONS **317** CITATIONS
SEE PROFILE

Jung-Hwan In
Gwangju Institute of Science and Technology
27 PUBLICATIONS **183** CITATIONS
SEE PROFILE

Effects of a sheath boundary on electron energy distribution in Ar/He dc magnetron discharges

Sang-Hun Seo, Jung-Hwan In, and Hong-Young Chang

Citation: Journal of Applied Physics **96**, 57 (2004); doi: 10.1063/1.1755850
View online: http://dx.doi.org/10.1063/1.1755850
View Table of Contents: http://scitation.aip.org/content/aip/journal/jap/96/1?ver=pdfcov
Published by the AIP Publishing

Effects of a sheath boundary on electron energy distribution in Ar/He dc magnetron discharges

Sang-Hun Seo,[a] Jung-Hwan In, and Hong-Young Chang
Low-Temperature Plasma Laboratory, Department of Physics, Korea Advanced Institute of Science and Technology, 373-1 Guseong-dong, Yuseong-gu, Daejeon, 305-701, Republic of Korea

(Received 27 October 2003; accepted 6 April 2004)

In this study, the effects of a sheath boundary on electron energy distribution and discharge characteristics in an unbalanced and planar-type dc magnetron sputtering system are investigated. The anode sheath potential is changed by applying dc bias voltages to the substrate. The electron energy distribution functions (EEDFs) are measured in argon and helium discharges using a single Langmuir probe in conjunction with the ac superposition method. The evolutions of the EEDFs are first observed in argon at 3 mTorr and then in helium at 30 mTorr. The results show that, as the substrate bias voltage decreases to high negative voltage, the EEDF transition from the bi-Maxwellian to the Maxwellian in the downstream region occurs at a specific bias voltage that depends on the operating gas. The major factors that affect the EEDF formation are investigated. In particular, the concept of total electron bounce frequency is introduced to represent the change of the sheath boundary condition. The observed EEDF transition is explained by comparing it with the plasma characteristic frequencies calculated from the measured EEDFs. As a result, the bi-Maxwellian distribution observed at the small substrate bias voltage is attributed to the low electron–electron collision frequency and the different loss mechanisms of two electron groups: the ambipolar diffusion loss of low-energy electron group confined by low plasma potential and the direct thermal loss of high-energy electron group, providing the electron current that compensates for the discharge current in a steady state.
[DOI: 10.1063/1.1755850]

I. INTRODUCTION

Unbalanced magnetron sputtering has been developed as a very simple and popular device for the deposition of metallic and dielectric thin films or the surface modification of the materials.[1,2] The annular magnetic field on the cathode enables the ionization rate to be enhanced by confining energetic electrons near the cathode, thereby ensuring an efficient sputtering rate even at low pressure. Low-pressure operation is preferred because it enables the high aspect ratio contact hole in microelectronic devices to be filled without a void. Moreover, by reducing the scattering of sputtered atoms in bulk plasma, the low pressure improves the efficiency of the deposition and the quality of the deposited film.[3,4]

The high-energy electrons confined by the magnetic field near a highly negatively biased cathode generate the high-density ions. These ions are accelerated through the high-voltage sheath formed in front of the cathode; they then impact the cathode, creating the sputtered atoms and the secondary electrons. The high-voltage sheath accelerates the secondary electrons that escape the magnetic trap near the cathode and consequently the discharge is sustained by these electrons. To balance the ion flux to the cathode, the electron flow from the cathode to the anode should be produced. In the downstream zone below the trap zone, the electron transport parallel to magnetic field owing to the strong limitation of the radial diffusion of electrons by the axial magnetic field can determine the discharge characteristics such as the spatial profiles of electron density and plasma potential over the whole discharge region.

An understanding of electron transport and kinetics is of great value for analyzing the process results and for further developing the magnetron system. Much of research on the characterization of magnetron plasma has been done with various diagnostic tools such as Langmuir probe,[5–9] laser-induced fluorescence,[10–12] and optical emission spectroscopy[13,14] as well as the theoretical approaches.[15–18] In particular, many valuable results have been acquired from the experiments associated with probe measurement. One interesting result is that the measured electron energy distribution functions (EEDF) is a non-Maxwellian distribution. Sheridan, Goeckner, and Goree analyzed the non-Maxwellian electron distribution with a two-temperature model. They showed that the non-Maxwellian electron distribution consists of the following: a low-energy electron group with a low electron temperature and a high density and a high-energy electron group with a high electron temperature and a low density.[6] They have also experimentally revealed the presence of strong electron drifts caused by the $\vec{E}\times\vec{B}$ drift near the trap region.[7]

The current-voltage ($I-V$) characteristic of a probe with two slopes (bi-Maxwellian) has been frequently observed in magnetron discharge. Unfortunately, the mechanism that causes the presence of the non-Maxwellian has not yet been elucidated, although some probable mechanisms have been suggested. One probable mechanism is Ramsauer effect,

[a]Electronic mail: SHSEO69@KAIST.AC.KR

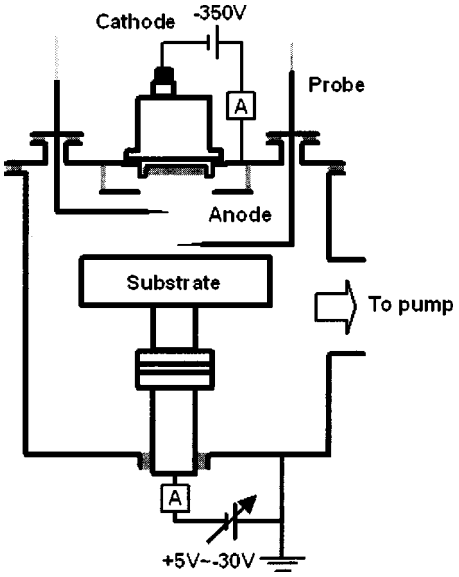

FIG. 1. Schematic diagram of an unbalanced dc magnetron sputtering system with a single Langmuir probe.

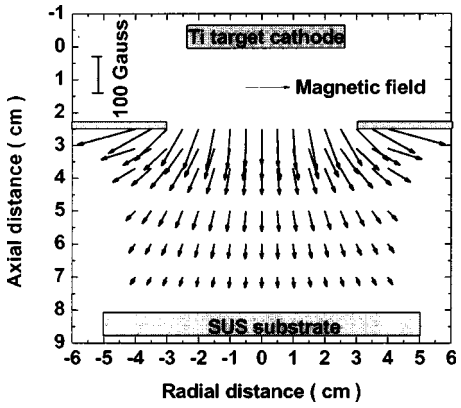

FIG. 2. Spatial distribution of the magnetic field in the chamber in the magnetron discharge system.

which represents the peculiar energy dependence of the collision cross section of neutral atom. However, this is an unacceptable explanation because, as we will show in this article, a bi-Maxwellian distribution can be observed even in a helium discharge, although the helium gas does not have the Ramsauer minimum. Another possible mechanism is that the sheath walls that are formed at the anode and cathode confine low-energy electrons whose energies are less than the potential of the sheath wall. Although such confinement effect is more likely, no direct proofs of this effect have been reported in detail.

In this article, we investigate the effects of the sheath wall on the EEDF formation and the discharge characteristics. By applying a dc voltage to the substrate, we can control the potential of the sheath wall. The evolutions of the EEDF against the substrate bias in argon and helium discharges are shown. To explain the observed EEDF features, we introduce a parameter of the electron total bounce frequency or the electron residence time, that can describe the change of the electron loss mechanism at sheath boundary and the influences of the electron collisions with neutrals and charged particles.

II. EXPERIMENTAL SETUP

Figure 1 shows the schematic diagram of a homemade magnetron sputtering system for the deposition of titanium film. The discharge chamber was evacuated by a diffusion oil pump supported by a mechanical pump. The base pressure was maintained below 10^{-5} Torr. The circular water-cooled titanium target with a diameter of 50 mm acted as a cathode of a glow discharge, and the disc-shaped anode embedded in the discharge chamber was located 25 mm from the cathode to ease the ignition of the discharge. Argon and helium gases were used to generate the plasma. Different operating pressures for each gas, 3 mTorr for the argon and 30 mTorr for the helium, were used because a stable discharge could be achieved even at low pressure of 3 mTorr for the argon discharge, whereas the ignition and stable maintenance of the discharge was very difficult at low pressures less than 30 mTorr for the helium discharge.

A high negative dc voltage ranging from -200 to -500 V could be applied to the cathode, and the anode was grounded with the discharge chamber. To achieve a similar electron density in both cases, the cathode voltage was adjusted. In this experiment, a dc voltage of -350 V was applied to the cathode for the argon discharge and -500 V was applied for the helium discharge. A stainless steel substrate with a diameter of 100 mm was mounted 80 mm from the cathode; it was biased by a dc voltage ranging from $+10$ to -100 V to control the potential of the sheath wall.

The magnetic field was measured with a magnetic Hall probe, and its spatial distribution in the downstream region is presented in Fig. 2. The intensity of the magnetic field at the surface of the cathode reaches about 300 G and decreases up to 100 G at the chamber center near the grounded anode. From Fig. 3, we can find that the magnetic field in the off-axis zone of the downstream region is very dispersive; the rapid increase of B_r and steep decrease of B_z as approaching the off-axis zone. The probe measurements were taken at the center of the discharge chamber and at the axial position 70

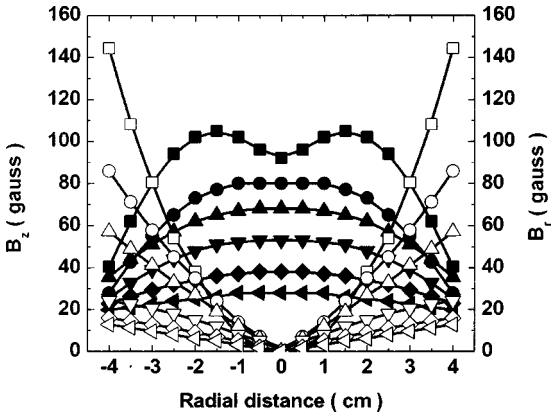

FIG. 3. Radial distribution of the axial (bold symbols) and radial (open symbols) components of the magnetic field at $z=2.5$ cm (■), 3 cm (●), 4 cm (▲), 5 cm (▼), 6 cm (♦), and 7 cm (◀).

mm from the cathode where the radial component of magnetic field is negligible.

The axially movable single Langmuir probe with a length of 4.5 mm and a diameter of 0.1 mm was installed at the top of the discharge chamber. The probe was bended into a L shape to enable measurements to be taken at the center of the discharge. To prevent the magnetic field from depleting the $I-V$ characteristic curve near the plasma potential, i.e., the low-energy part of EEDF by the influence of the magnetic field, the radius of the probe R has to be always smaller than the Larmor radius of the electron r_{ce}, i.e., $R \ll r_{ce}$. Because r_{ce} of an electron with an energy of 1 eV was about 0.11 mm under the strongest magnetic field of 300 G in our discharge, the probe measurement with $R=0.05$ mm was reliable throughout the entire discharge region. Furthermore, when R was 0.05 mm, the probe can resolve electrons with energy less than 0.1 eV in the downstream region where the intensity of magnetic field was less than 100 G.

The ac superposition technique was used to obtain the second derivative of the $I-V$ characteristic that is directly related to the EEDF. The plasma parameters such as plasma potential (V_p), electron density (n_e), and effective electron temperature (T_{eff}) were determined from the obtained second derivatives of the probe $I-V$ curves. The plasma potential was found from the minimum point of the absolute value of the second derivative of probe current, and the electron density and the effective electron temperature were calculated from the integrals of the EEDF as follows:

$$n_e = \int_0^{\varepsilon_{\max}} g_e(\varepsilon)\, d\varepsilon, \tag{1}$$

$$T_{\text{eff}} = \frac{2}{3}\langle\varepsilon\rangle = \frac{2e}{3n_e}\int_0^{\varepsilon_{\max}} \varepsilon g_e(\varepsilon)\, d\varepsilon'. \tag{2}$$

where $g_e(\varepsilon)$ is the EEDF and $\varepsilon_{\max}$ is determined by the dynamic range of the EEDF measurement. In addition, the currents that flowed to the substrate and the cathode were monitored *in situ* to investigate the variation in the loss balance of charged particles against the change of the substrate bias voltage.

III. EXPERIMENTAL RESULTS

A. Argon discharge

Figure 4 contrasts the evolution of the electron energy probability function [EEPF, $f_e(\varepsilon)=\varepsilon^{-1/2}g_e(\varepsilon)$] in argon discharge against the substrate bias voltage (V_S) which ranged from $+5$ to -30 V. For $V_S \geqslant 0$ V, the measured EEPFs show a bi-Maxwellian distribution typically observed in magnetron discharges. Using the two-temperature model, the bi-Maxwellian EEPF can be resolved as two Maxwellian EEPFs with the electron temperatures of T_{el} and T_{eh} and the electron density of n_{el} and n_{el}, respectively as follows:

$$f_p(\varepsilon) = \frac{2}{\sqrt{\pi}}[n_{\text{el}}T_{\text{el}}^{-3/2}\exp(-\varepsilon/T_{\text{el}}) + n_{\text{eh}}T_{\text{eh}}^{-3/2} \times \exp(-\varepsilon/T_{\text{eh}})]. \tag{3}$$

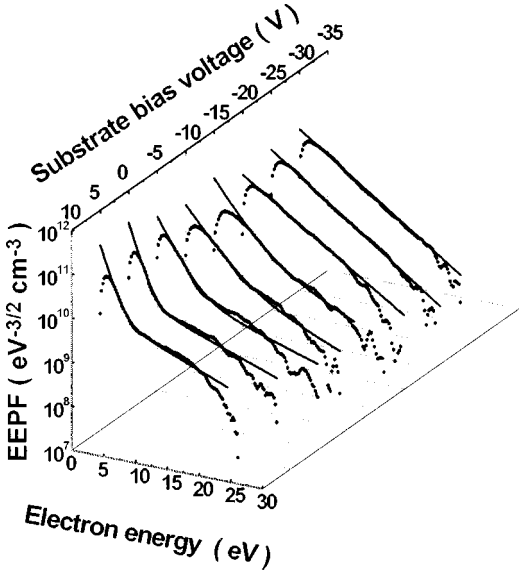

FIG. 4. The evolution of the EEPF against the substrate bias voltage in the argon discharge at a target voltage of -350 V and an operating pressure of 3 mTorr. The solid lines on the data are the fitting curves.

The four fitting parameters of n_{el}, n_{eh}, T_{el}, and T_{eh} were obtained from a successive fitting procedure until the chi-square value reached its minimum value. We could determine, for example, that the EEPF consisted of the low-energy group with $T_{\text{el}} \sim 0.97$ eV and $n_{\text{el}} = 8.0\times10^{10}/\text{cm}^3$ and the high-energy group with $T_{\text{eh}} \sim 8.4$ eV and $n_{\text{eh}} = 4.4\times10^{10}/\text{cm}^3$ for $V_S = 0$ V. Bulk plasma therefore consists of a background low-energy electron group with a high density and a low temperature, along with a high-energy electron tail with low density and a high temperature for the grounded substrate boundary.

Interestingly, a gradual transition of the EEPF occurs from a bi-Maxwellian distribution to a Maxwellian distribution as V_S decreases from a positive value to a negative value. The change in the EEPF feature is scarcely noticeable for $V_S \geqslant 0$ V, and the bi-Maxwellian EEPF is held. However, the EEPF feature in the elastic energy part of $\varepsilon < \varepsilon^*$ ($=11.6$ eV) begins to change intensively as V_S decreases below 0 V, as shown in Fig. 4.

Considering the variations of the plasma and discharge parameters against V_S, we can divide V_S into three regions. In the first region, $V_S \geqslant 0$ V and the EEPFs can be characterized as a bi-Maxwellian distribution. As V_S increases in this V_S region, n_e decreases and T_{eff} increases slightly, as shown in Fig. 5(a). In addition, it can be found that V_S significantly affects the substrate current I_S and the cathode target current I_C but $|I_C| \approx |I_S|$, as shown in Fig. 5(b).

We also observed that V_p rapidly increases as V_S increases, though no change occurs in the sheath wall potential that is formed in front of the substrate ($\phi_w = V_p - V_S$) because $\Delta V_S \cong \Delta V_p$; V_p remains constant at about 2 V in this V_S region. However, the sheath potential ($\phi_c = V_p - V_C$, where the V_C is the cathode voltage) that is developed in front of the cathode becomes higher because of the rapid increase of V_p, thereby increasing I_C. Considering $|I_C| \approx |I_S|$ in this V_S region, we can deduce that the ion flux to

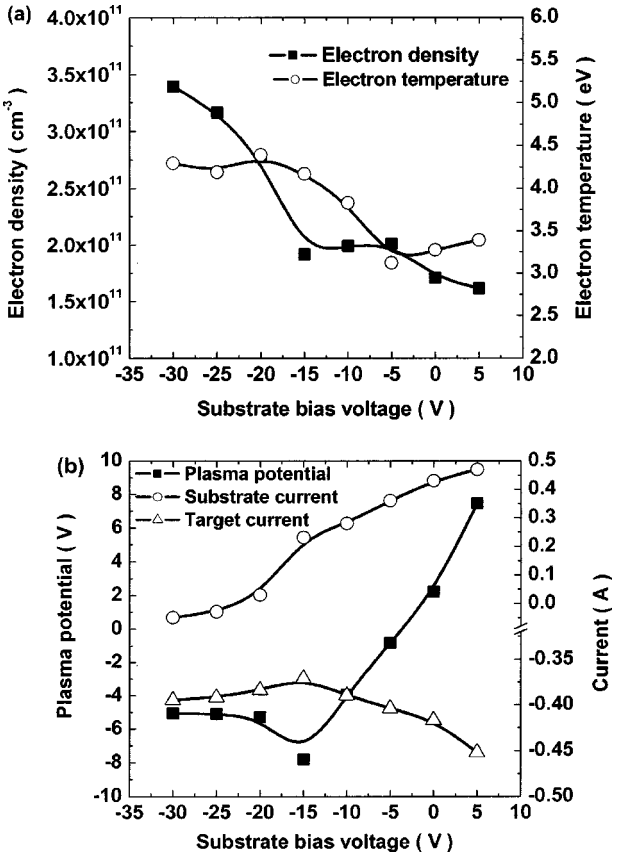

FIG. 5. (a) The electron density and the effective electron temperature and (b) the plasma potential and the substrate and target currents vs the substrate bias in the argon discharge.

the cathode I_C is primarily balanced by the electron loss to the substrate I_S. As a result, I_S must increase even though ϕ_w remains constant, resulting in the decrease of n_e with increasing V_S.

In the second V_S region of $-15\,\mathrm{V} \leqslant V_S \leqslant -5\,\mathrm{V}$, the outstanding change of the EEPF progresses, especially in the elastic energy range. As shown in Fig. 5(a), the characteristics of this V_S region are the constancy of n_e and the rapid increase in T_{eff}. We could find from Fig. 4 that T_{el} increases and T_{eh} slowly decreases with the reduction of the peak of the low-energy electron group. The plasma potential still decreases linearly as V_S decreases, but its decrement is smaller than that of V_S, that is, $|\Delta V_S| > |\Delta V_p|$. As a result, ϕ_w gradually increases to about 7 V at $V_S = -15\,\mathrm{V}$. The increase of ϕ_w causes the electron loss in the substrate to decrease through the sheath wall confining more energetic electrons. A lot of energetic electrons with $\varepsilon < e\phi_w (\approx 7\,\mathrm{eV})$ is allowed to stay longer in bulk plasma and experience the electron–electron collision with cold electrons by the increased ϕ_w. Participation of more energetic electrons in the energy relaxation process of cold electrons gives rise to the increase of T_{el}, resulting in the increase of T_{eff}. In addition, the decrease of the electron loss in the substrate with decreasing V_S is accompanied with the reduction of I_S. The reduction of I_C accompanied with the decrease of I_S causes n_e to be a constant. However, note that I_C is not fully balanced exclusively by I_C; that is, $|I_S| < |I_C|$ in this region, as shown in Fig. 5(b).

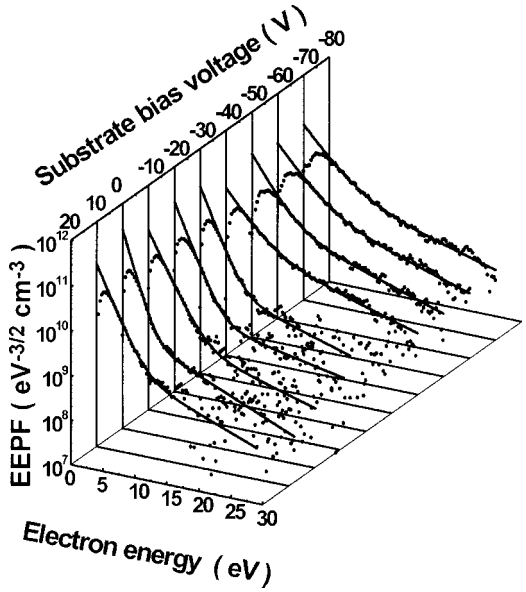

FIG. 6. The evolution of the EEPF against the substrate bias voltage in the helium discharge at a target voltage of -500 V and an operating pressure of 30 mTorr.

In other words, other paths for the electron loss, such as the anode or the chamber wall, begin to work.

In the third V_S region in which the substrate is highly negatively biased ($\geqslant -20$ V), the EEPF evolves to a complete Maxwellian distribution. Contrary to the case in the second V_S region, n_e steadily increases as V_S decreases, while T_{eff} becomes higher ($\approx$4.2 eV) after the EEPF evolves into the Maxwellian distribution and then, remains almost constant irrespective of V_S. The plasma potential, even if it slightly increases the moment V_S is changed from -15 to -20 V, remains constant at about -5 V at $V_S < -20$ V. Thus ϕ_w continues to increase, following the change of V_S. The cathode current is insensitive to the change of V_S in this V_S region, and seems to be saturated with the current density of about $-20\,\mathrm{mA/cm^2}$. On the other hand, I_S becomes almost zero during this EEPF transition at $V_S = -20$ V and even has a negative value as V_S decreases further. It implies the change in the role of the substrate from a major path for electron loss for small V_S to a path for ion loss for high negative V_S. Moreover, since the electrons trapped between the cathode sheath and the substrate sheath have more chances to collide with neutrals, their cross-field diffusion is enhanced. We could obviously observe that the plasma expands radially and its emission fills the whole discharge chamber.

B. Helium discharge

As mentioned previously, because the breakdown of the helium discharge at low pressures was very difficult for the helium discharge due to its higher ionization threshold energy of 24.6 eV, we inevitably increased the operating pressure and could achieve the stable discharge at the pressures higher than 30 mTorr. Figure 6 shows the evolution of the EEPF against V_S in the helium discharge at 30 mTorr. Just as in the case of the argon discharge, we could observe the

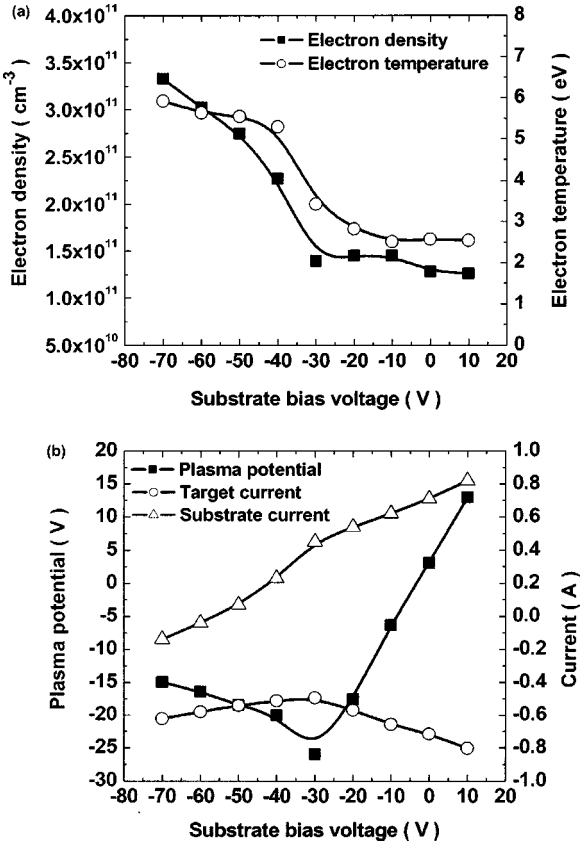

FIG. 7. (a) The electron density and the effective electron temperature and (b) the plasma potential and the substrate and target currents vs the substrate bias in helium discharge.

appearance of a bi-Maxwellian EEPF for small V_S and the EEPF transition from a bi-Maxwellian distribution to an almost Maxwellian distribution at a specific V_S. But, we could find that this transition in the helium discharge occurs at higher V_S of -40 V.

Figure 7 shows the variations of the discharge and plasma parameters against V_S. The trends of variation of these parameters are very similar to those in the argon discharge, except for the shift of the critical V_S. In the helium discharge, the first region corresponds to $V_S \geqslant 0$ V, the second region comes under $-10\,\mathrm{V} \leqslant V_S \leqslant -30\,\mathrm{V}$, and the third region fall under $V_S \geqslant -40$ V. In the transition region of the second V_S region, the electron thermalization in the elastic energy range of the EEPF in the helium discharge does not occur as actively as that in the argon discharge. As a result, the EEPF does not become a complete Maxwellian distribution with this transition as shown in Fig. 6. Nevertheless, it is evident that the significant changes of the EEPF feature and the plasma and discharge parameters happen as V_S is changed.

C. Sheath boundary condition and the total electron bounce frequency

In a weakly ionized low-pressure discharge, electron collisions with neutral atoms are more frequent than collisions between charged particles. However, because the electron energy relaxation length λ^* is comparable to or higher than the plasma dimension L in low-pressure regime and the spatial displacement of electrons occurs rapidly compared to the total energy change due to collisions and heating, these electrons encounter a sheath boundary before experiencing the significant energy change. Depending on the sheath potential energy ($e\phi_{sw}$), they are scattered back ($\varepsilon < e\phi_{sw}$) or are lost in the sheath ($\varepsilon > e\phi_{sw}$). The electrons reflected at the sheath edge have more chance to lose their energies through the inelastic collisions with neutral atoms or the electron–electron collision. Thus the condition of the sheath boundary is definitely important in determining the electron energy distribution in bulk plasma. Furthermore, an interesting fact is that the plasma potential at sheath edge is very low with a few volts in our magnetron discharge, although it is relatively high with a few tens of volts in conventional discharges.

In the elastic energy range of $\varepsilon < \varepsilon^*$, where ε^* is the first excitation energy of the neutral atom, the electrons experience almost elastic collisions with neutral atoms, that is, quasielastic collisions. The quasielastic collisions include collisions with a small energy loss compared to electron kinetic energy. They are characterized by the parameter ζ, which is the average fraction of the energy lost in a single collision. The electron-neutral collision frequency is written as

$$\nu_{\mathrm{en}} = N k_{\mathrm{en}}(T_e), \tag{4}$$

where $N[=8.32\times10^{11} p\,(\mathrm{mTorr})/T_N\,(\mathrm{eV})/\mathrm{cm}^3]$ is the number of neutral atoms and $k_{\mathrm{en}}(=\sigma_{\mathrm{en}}\upsilon_e)$ rate constant.[19] Because $\zeta(=2m_e/M \sim 10^{-4}$ for helium gas) $\ll 1$, the energy relaxation frequency through the electron-neutral momentum transfer collision ν_M $(=\zeta\nu_{\mathrm{en}} \ll \nu_{\mathrm{ee}}$ even though $\nu_{\mathrm{en}} \gg \nu_{\mathrm{ee}}$. As a result, the effect of the electron-neutral momentum transfer collision on the determination of the EEPF feature can be neglected. Another important collision process that seriously affects the EEPF formation is the electron–electron collision process. The sufficiently frequent electron–electron collisions tend to transform the EEPF into a Maxwellian distribution. The electron–electron collision frequency depends on such plasma parameters as n_e and T_e and can be written as[19]

$$\nu_{\mathrm{ee}} = 2.91\times10^{-6} n_e T_e^{-3/2} \ln\Lambda, \tag{5}$$

where ν_{ee} is the electron-electron collision frequency and $\ln\Lambda$ is the Coulomb logarithm.

In the inelastic energy range of $\varepsilon \geqslant \varepsilon^*$, inelastic collisions (excitation and ionization) with neutral atoms are more frequent than other elastic collisions and consequently the rapid depletion in the electron energy distribution occurs around the threshold energy. For the electrons with $\varepsilon \geqslant \varepsilon^*$, which however are trapped by sheath potential (i.e., $e\phi_w > \varepsilon^*$), their bounce motion becomes important, because it gives the electrons more chances to undergo the inelastic collision with a neutral atom in the bulk plasma if the mean free path for the electron loss becomes longer than the electron energy relaxation length due to the confinement effect of the high-voltage sheath.

As a parameter which can indicate the change of the electron loss through the sheath potential wall, we suggest

the total electron bounce frequency ν_l ($\equiv 1/\tau_l$, where τ_l is the electron residence time). The total electron bounce frequency can be defined as the total number of bounces between sheath boundaries until electrons escape from the bulk plasma.[19] Assuming the trapped electrons do not experience the significant energy relaxation collisions within the plasma bulk ($\lambda^* \gg L$), the typical loss velocity of the plasma at the plasma-sheath boundaries is the Bohm velocity ($v_B = \sqrt{T_e/M}$). Thus the electrons bounce v_{th}/v_B times until their loss and then, the total mean free path of the electrons for their loss λ_l is $2L(v_{\text{th}}/v_B)$. Therefore, the residence time of the electrons defined by $\tau_l = \lambda_l / v_{\text{th}}$ is $2L/v_B$. On the other hand, because the free electrons with $\varepsilon \geqslant \phi_w$ easily overcome the sheath potential barrier when they arrive at the sheath wall, the maximum λ_l is $2L$ and then, their residence time is therefore $2L/v_{\text{th}}$. As a result, the total electron bounce frequency for an electron, depending on its energy, can be represented by

$$\nu_l = \begin{cases} v_B/2L & \text{for } \varepsilon \leqslant e\phi_w \\ v_{\text{th}}/2L & \text{for } \varepsilon \geqslant e\phi_w \end{cases}. \tag{6}$$

Such characteristic frequencies as the ionization frequency ν_{iz}, the excitation frequency ν^*, and the electron-electron collision frequency ν_{ee}, together with the total electron bounce frequency ν_l, directly affect the EEPF feature. The quantities ν_{en}, ν_{ee}, and ν_l were obtained from the Eqs. (4), (5), and (6), respectively and ν_{iz} and ν^* were calculated as the integrals of the measured EEPFs with the corresponding cross sections as follows:

$$\nu_\alpha = Nk_\alpha = N\langle \sigma_\alpha v_e \rangle = \frac{N}{n_e} \int_0^{\varepsilon_{\max}} \sigma_\alpha v_e g(\varepsilon) d\varepsilon, \tag{7}$$

where σ_α is the cross-section for excitation or ionization, and v_e is the electron thermal velocity.

IV. DISCUSSION

As shown in Figs. 4 and 6, the EEPF transitions to the Maxwellian distribution occur at a different specific V_S (V_{CS}), depending on the operating gas. The potential of the sheath wall, however, commonly becomes higher than the first excitation energy of each gas when the transitions are completed as described in Fig. 8. As V_S further decreases below V_{SC}, the sheath potential keeps increasing, so that it becomes a specular boundary for all electrons detected by the probe. There is a difference of the trend of the ϕ_w evolution in the second V_S region ($V_{SC} < V_S < 0$ V) between the argon discharge and the helium discharge. The sheath potential, even if insignificant, increases as V_S decreases. This different evolution of ϕ_w is reflected in the evolution of the EEPF. The electron energy thermalization between the low-energy electron group and the high-energy electron group in the elastic energy range is active in the second V_S region for the argon discharge (see Fig. 4) but is indistinct for the helium discharge (see Fig. 6). This phenomenon is due to the lower ν_{ee} in helium plasma.

As mentioned previously, the electron–electron collision plays an major role in the electron energy relaxation in the elastic energy range of the EEPF ($\varepsilon < \varepsilon^*$). The τ_l can become

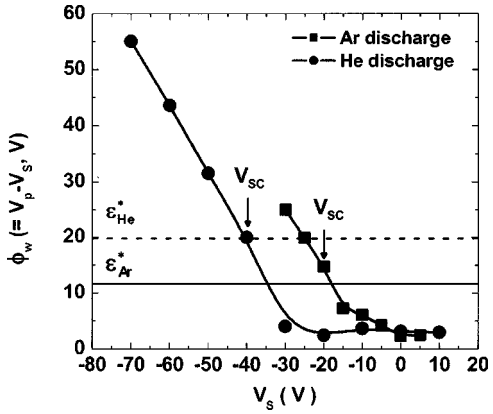

FIG. 8. The evolution of the sheath wall potential against the substrate bias voltage. The first excitation energy levels of the argon and helium atoms are represented and the arrows at $V_S = -20$ and -40 V denote the occurrence of the EEPF transition in the argon and helium plasmas, respectively.

a gauge to determine whether the EEPF becomes a Maxwellian distribution or not in the elastic energy range. If $\tau_l \nu_{\text{ee}} \ll 1$, electrons rarely undergo the electron–electron collisions during τ_l, so that the active thermalization of electron energy cannot be expected. In the opposite case ($\tau_l \nu_{\text{ee}} \gg 1$), however, electrons collide at least once with each other during τ_l. It implies that the thermalization of electron energy occurs actively, so that the EEPF can evolve into a Maxwellian distribution.

In the first and the second V_S regions ($V_S > V_{SC}$) of the argon and helium discharges, the electrons with $\varepsilon < \varepsilon^*$ are governed by two characteristic residence times. In other words, the electron loss at the sheath boundary is determined by the different mechanism depending on the electron energy. The characteristic residence time of the trapped electrons with $\varepsilon < e\phi_w$ is $\tau_{ll} (= 1/\nu_{ll})$, which is represented with $2L/v_B$ from Eq. (6). On the other hand, the electrons with $e\phi_w < \varepsilon < \varepsilon^*$ are governed by the $\tau_{lh} (= 1/\nu_{lh})$, which is represented with $2L/v_{\text{th}}$.

Figure 9 shows the bifurcation of τ_l in the first and second V_S regions with the plasma characteristic frequencies obtained from the Eqs. (4), (5), and (7). Here, τ_{ll} was calculated from $2L(T_{\text{el}}/M)^{-1/2}$ and τ_{lh} was calculated from $2L(8T_{\text{eh}}/\pi m)^{-1/2}$. Because $\tau_{ll}\nu_{\text{ee}} \gg 1$ for the trapped electrons, the electrons actively interact with other trapped electrons and then, generate a low-energy Maxwellian group. On the other hand, because the relatively high-energy electrons with $e\phi_w < \varepsilon < \varepsilon^*$ have a very short residence time, that is, $\tau_{lh}\nu_{\text{ee}} \ll 1$, they are lost on arrival at the sheath edge without undergoing the collisions with other electrons. Therefore, under these plasma conditions, the bifurcation of the electron loss mechanism at sheath boundary leads to a bi-Maxwellian EEPF with a low-energy electron group.

Meanwhile, the characteristic residence time of the electrons with $\varepsilon < \varepsilon^*$ in the third V_S region can be represented by a single characteristic residence time τ_l, which is expressed as $2L(T_{\text{eff}}/M)^{-1/2}$, because all electrons in the elastic energy range are trapped by the sheath wall. Furthermore, since $\tau_l \nu_{\text{ee}} \gg 1$, as shown in Fig. 9, the electron energy thermalization occurs actively and the EEPF tends to become a Max-

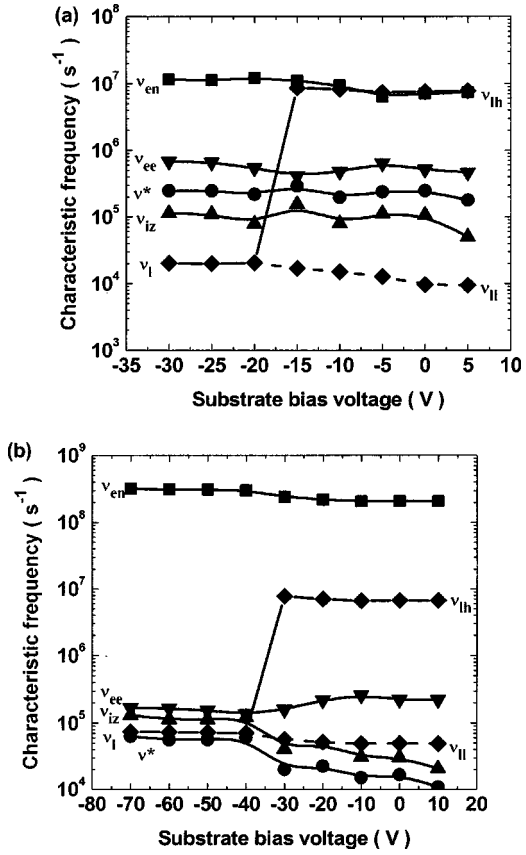

FIG. 9. The variation trends of the characteristic frequencies (ν_{en}, ν_{ee}, ν^*, and ν_{iz}) and the total electron bounce frequency (ν_l) against the substrate bias voltage in (a) the argon discharge and (b) the helium discharge.

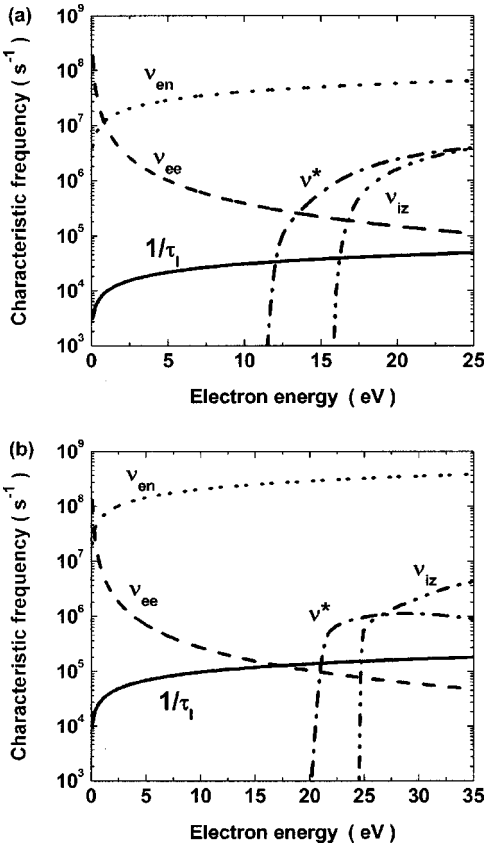

FIG. 10. The characteristic frequencies (ν_{en}, ν_{ee}, ν^*, and ν_{iz}) and the total electron bounced frequency ($1/\tau_l$) against the electron energy in (a) the argon discharge and (b) the helium discharge.

wellian distribution. We can also deduce that since ν_{ee} in the helium discharge is lower than that in argon discharge, the electron energy thermalization is relatively slow. As a result, in spite of the development of high-voltage sheath enough to confine all electrons in the elastic energy range within the bulk plasma, the EEPF does not evolve into a complete Maxwellian distribution in the helium discharge as rapidly as in the argon discharge.

For the electrons in the inelastic energy range ($\varepsilon > \varepsilon^*$), the major energy relaxation process is the inelastic collision with neutral atoms because ν^*, $\nu_{iz} \gg \nu_{ee}$ in this energy range, as shown in Fig. 10. This type of energy relaxation rarely occurs in the first and the second V_S regions because the energy relaxation length is very longer than the discharge dimension; as a result, they overcome the sheath wall potential and are directly lost in the substrate. However, the energy relaxation of these high-energy electrons is significant in the bulk plasma when the sheath potential is larger than their energy levels. Moreover, the ionization of high-energy electrons within the bulk plasma is expected when $e\phi_w > \varepsilon_{iz}$ because the residence time of these electrons is so long that they collide with neutral atom at least once ($\tau_l \nu_{iz} \gg 1$). This bulk cooling of high-energy electrons will changes the spatial profile of n_e.

V. CONCLUSIONS

We investigated the effects of the sheath boundary condition on the EEPF in magnetron argon and helium discharges. The EEPF transitions from a bi-Maxwellian distribution to a Maxwellian distribution clearly occur at the critical substrate bias voltages at which the sheath wall potentials become higher than the first excitation energies of argon and helium atoms. We introduced the concept of the total electron bounce frequency, i.e., the electron residence time that reflects the change in the electron loss mechanism against the change in the sheath wall potential. Through this concept, we explain the change of the EEPF feature, especially the formation of the bi-Maxwellian distribution, in a magnetron discharge with a very low plasma potential. These results give a decisive clue in explaining the appearance of the bi-Maxwellian distribution in magnetron discharges.

ACKNOWLEDGMENT

The authors would like to thank the National Research Laboratory (Grant no. M10104000071-02J0000-03011) and the Engineering and Research Center (Grant no. R11-2000-086-03007-0) for their financial support of this research.

[1] B. Window and N. Savvides, J. Vac. Sci. Technol. A **4**, 196 (1986).
[2] M. J. Jung, K. H. Nam, L. R. Shaginyan, and J. G. Han, Thin Solid Films **435**, 145 (2003).
[3] S. L. Rohde, I. Petrov, W. D. Sproul, S. A. Barnett, P. J. Rudnik, and M. E. Graham, Thin Solid Films **193/194**, 117 (1990).
[4] R. P. Howson, H. A. J'afer, and A. G. Spencer, Thin Solid Films **193/194**, 127 (1990).
[5] S. M. Rossnagel and H. R. Kaufmann, J. Vac. Sci. Technol. A **4**, 1822 (1986).

[6] T. E. Sheridan, M. J. Goeckner, and J. Goree, J. Vac. Sci. Technol. A **9**, 688 (1991).
[7] T. E. Sheridan, M. J. Goeckner, and J. Goree, J. Vac. Sci. Technol. A **16**, 2173 (1998).
[8] P. Špatenka, J. Vlček, and J. Blažek, Vacuum **55**, 165 (1999).
[9] D. J. Field, S. K. Dew, and R. E. Burrell, J. Vac. Sci. Technol. A **20**, 2032 (2002).
[10] M. J. Goeckner, J. Goree, and T. E. Sheridan, J. Vac. Sci. Technol. A **8**, 3920 (1990).
[11] M. J. Goeckner, J. Goree, and T. E. Sheridan, IEEE Trans. Plasma Sci. **19**, 301 (1991).
[12] Y. W. Choi, M. Bowden, and K. Muraoka, Jpn. J. Appl. Phys., Part 1 **35**, 5858 (1996).
[13] L. Gu and M. A. Lieberman, J. Vac. Sci. Technol. A **6**, 2960 (1988).
[14] S. Miyake, N. Shimura, T. Makabe, and A. Itoh, J. Vac. Sci. Technol. A **10**, 1135 (1992).
[15] T. E. Sheridan, M. J. Goeckner, and J. Goree, J. Vac. Sci. Technol. A **8**, 30 (1990).
[16] J. E. Miranda, M. J. Goeckner, J. Goree, and T. E. Sheridan, J. Vac. Sci. Technol. A **8**, 1627 (1990).
[17] S. Ido and K. Nakamura, Jpn. J. Appl. Phys., Part 1 **32**, 5698 (1993).
[18] E. Shidoji, M. Nemoto, T. Nomura, and Y. Yoshikawa, Jpn. J. Appl. Phys., Part 1 **33**, 4281 (1994).
[19] S. H. Seo, C. W. Chung, J. I. Hong, and H. Y. Chang, Phys. Rev. E **62**, 7155 (2000).